

Syntheses and characterization of novel asymmetric bent-core mesogens exhibiting polar smectic phases

Kinga Gomola,^{ab} Lingfeng Guo,^a Surajit Dhara,^{ac} Yoshio Shimbo,^a Ewa Gorecka,^b Damian Pocięcha,^b Jozef Mieczkowski^b and Hideo Takezoe^a

Received 17th November 2008, Accepted 3rd April 2009

First published as an Advance Article on the web 11th May 2009

DOI: 10.1039/b820566c

Three series of asymmetric bent-core compounds were synthesized and their mesomorphic properties were studied. All the compounds possess 2-methylresorcinol as a central unit and a stilbene bridge as a main element in the structure. Molecules of series I and series II possess only saturated terminal chains while those of series III have one or both unsaturated chain/s. The mesophases were characterized by using optical polarizing microscopy, differential scanning calorimetry, X-ray diffraction, electrooptic and dielectric measurements, and miscibility studies. All the compounds exhibit the isotropic to SmAP_R phase transition and the B_{1RevTilted} phase at lower temperatures. For compounds with one olefinic terminal chain, the temperature range of the SmAP_R phase was found to be narrower in comparison to compounds with both saturated terminal chains. A detailed dielectric investigation was carried out on both the SmAP_R and B_{1RevTilted} phases and two different types of dynamical behaviour were observed.

1. Introduction

Liquid crystalline phases exhibited by compounds composed of bent-core molecules have been an important subfield of liquid crystals because of their great interest in academia and their growing potential in display applications.¹ The occurrence of spontaneous polarization resulting from the polar packing of the bent molecules in the smectic layers that is permitted by the symmetry² made the subject more interesting from the fundamental point of view. The most frequently observed smectic phase exhibited by bent-shaped molecules is the B₂ or SmCP phase in which the molecules are tilted with respect to the layer normal. This phase may be regarded as the polar variant of the SmC phase, with C₂ symmetry. Depending on the stacking of the smectic layers and the arrangement of the molecules in the layers, the SmCP phase may exhibit antiferroelectric or ferroelectric properties. In some rare cases the polarly ordered molecules are, on average, aligned orthogonal with respect to the layer planes and a polar interdigitated biaxial SmA (SmA_{db}) phase results.³ It is designated as SmAP, when polar switching is possible, and SmAP_A when an antiferroelectric order exists in neighboring layers.⁴ Recently we found a polar non-tilted smectic phase, SmAP_R, with random polarization.^{5–7} This phase appears as uniaxial and nonpolar in the absence of an electric field, but the polar order can be easily induced by the application of a weak field.⁸

Very recently we also reported a novel display mode that can be realised in the SmAP_R phase.⁹ The most important advantages of this mode in the SmAP_R phase are the fast response time

(~100 μs), essentially no threshold voltage followed by continuous transmittance change, the high contrast ratio (3000:1), and the wide viewing angle.⁹ To realise practical display applications, however, we have to solve a number of problems related to: wider temperature range of SmAP_R including room temperature, larger biaxiality, lower operating voltages, stable layer structure, etc. So far only one homologous series of compounds exhibiting SmAP_R is known. So the most urgent issue is to synthesize a variety of compounds which show the SmAP_R phase and characterize their mesogenic properties and display performance. In this paper we report the synthesis of three series of novel bent-core asymmetric compounds in which the lack of symmetry is derived from different lateral substituents and differences in the terminal alkoxy chain lengths; and also in some compounds there are different carbon-carbon double bonds in one or both of the terminal chains. It is expected that the introduction of the above structural modifications may result in the decrease of the melting transition temperature and wider range of the SmAP_R phase. Indeed, we observed the expected result in the transition temperature but not in the temperature range; *i.e.*, in the compounds with one olefinic terminal chain, the isotropization temperatures decreased and the SmAP_R phase appeared in slightly narrower temperature ranges in comparison to compounds with both saturated terminal chains. On the other hand the SmAP_R phase was destabilized for most of the pure compounds possessing unsaturated chains at both branches.

2. Results and discussion

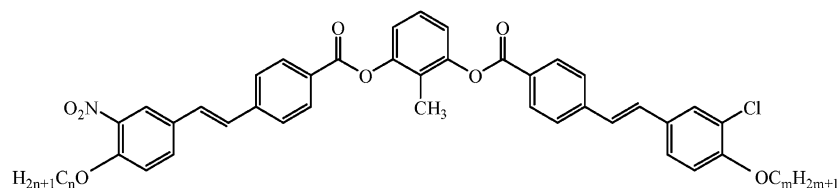
Let us first show mesomorphic properties of the synthesized compounds of series I, II and III. The transition temperatures and associated enthalpies of the compounds of series I (**12-NCl-m**) and in series II (**14-NCl-m**) are summarized in Table 1. Numbers at both sides of the sample names stand for the

^aDepartment of Organic and Polymeric Materials, Tokyo Institute of Technology, O-okayama, Meguro-ku, Tokyo, 152-8552, Japan

^bChemistry Department, Warsaw University, Al. Zwirki i Wigury 101, 02-089 Warsaw, Poland

^cSchool of Physics, University of Hyderabad, 500046, India

Table 1 Phase transition temperatures (°C) and corresponding enthalpies [J g⁻¹] for compounds of series I (n = 12) and series II (n = 14). Numbers at both sides of the sample names stand for the numbers of carbons in both end chains. N and Cl stand for substituents NO₂ and Cl at the left and right wings, respectively



Sample name	Cr	$B_{1\text{RevTilted}}$	SmAP _R	Iso	ΔT (SmAP _R)
12-NCl-5	• 104.36 [18.06]	• 113.03 [10.92]		•	—
12-NCl-7	• 92.45 [13.68]	• 125.93 [12.95]		•	—
12-NCl-8	• 80.85 [8.75]	• 127.61 [0.21]	• 129.95 [12.96]	•	2.34
12-NCl-10 ⁷	• 123.24 [24.70]	• 128.30 [0.40]	• 134.60 [9.72]	•	16.30
12-NCl-11	• 100.72 [45.50]	• 125.02 [0.55]	• 135.45 [10.59]	•	10.43
12-NCl-12 ⁵⁻⁷	• 121.00 [15.70]	• 125.90 [0.61]	• 136.80 [10.80]	•	10.90
12-NCl-13 ⁷	• 103.30 [43.90]	• 123.30 [0.20]	• 136.30 [6.60]	•	13.00
12-NCl-14	• 107.00 [51.72]	• 124.92 [0.66]	• 137.96 [10.53]	•	13.04
12-NCl-15 ⁷	• 97.76 [50.19]	• 123.25 [0.40]	• 136.50 [10.15]	•	13.25
12-NCl-16	• 118.00 [23.12]	• 125.97 [0.99]	• 140.06 [9.77]	•	14.09
12-NCl-18 ⁷	• 113.71 [20.89]	• 121.39 [0.20]	• 134.72 [8.40]	•	13.33
14-NCl-13	• 102.77 [38.58]	• 126.81 [0.85]	• 139.24 [9.01]	•	12.43
14-NCl-14 ^{5,6,8}	• 116.53 [22.06]	• 127.72 [1.00]	• 141.27 [9.08]	•	13.55
14-NCl-15 ⁷	• 117.70 [21.27]	• 126.70 [0.86]	• 140.93 [8.70]	•	14.23
14-NCl-16	• 116.40 [22.47]	• 125.31 [0.85]	• 140.88 [8.55]	•	15.57

numbers of carbon in both end chains. N and Cl stand for substituents NO₂ and Cl at left and right wings, respectively. A few materials from series I and II have already been studied and characterized by Pocięcha *et al.*^{6,7} and Shimbo *et al.*^{8,9} Asymmetry in the molecular structure in both of these series arises from different lateral substituents and different lengths of saturated terminal chains except for **12-NCl-12** and **14-NCl-14** where asymmetry is derived only from the different substituents. The molecules of series I possess one unchanged dodecyloxy group connected to one of the arms, while the length of the second terminal chain was varied. The short-tailed homologues **12-NCl-5** and **12-NCl-7** form exclusively $B_{1\text{RevTilted}}$, the columnar phase made of layer fragments with 2D density modulation in the plane perpendicular to the polarization direction.¹⁰ Compounds with middle and long terminal chains show two enantiotropic mesophases: a lower temperature $B_{1\text{RevTilted}}$ phase and a higher temperature SmAP_R phase with uniaxial optical properties, as confirmed by conoscopic measurements.⁶ Introduction of a tetradecyloxy group as a terminal chain in series II (**14-NCl-m**) resulted in only slightly increased isotropization temperature and did not influence the range of the SmAP_R mesophase during the variations of length of the second tail.

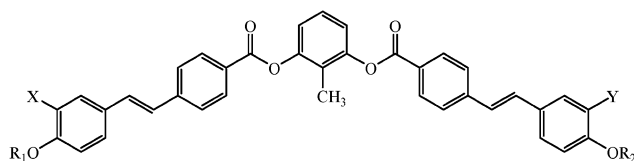
Table 2 summarizes the transition temperatures and associated enthalpies for final compounds (series III) with olefinic double bond(s) in one or both the terminal chain(s). Nomenclature of the sample names follows the same rules as for series I and II, except for **d** which indicates the existence of double bond(s). All asymmetric bent-core compounds exhibit enantiotropic SmAP_R and monotropic $B_{1\text{RevTilted}}$ phases except for two compounds: **11-NCl-11d** with undecenyloxy and undecyloxy terminal groups and **11d-NCl-11d** with two unsaturated terminal chains, which show no liquid crystalline phases. Introduction of a vinyl group

at the end of a terminal chain decreases the temperatures range of SmAP_R, but does not broaden the range of mesophase. Also the $B_{1\text{RevTilted}}$ phase is supercooled and exists even at room temperature. The presence of vinyl group at the end of the terminal chain, connected to the arm with chlorine **14-NCl-11d**, resulted in similar properties comparing to compounds possessing a terminal double bond connected to the arm with a nitro group **11d-NCl-14**.

We performed X-ray diffraction measurements in the SmAP_R phase as well as in the $B_{1\text{RevTilted}}$ phase on unoriented samples. For the compound **11d-NCl-14** in the SmAP_R phase, two commensurate reflections could be seen in the small angle region indicating a smectic ordering of the mesophase as shown in Fig. 1. The layer spacing d gradually increases as the temperature is lowered in the SmAP_R phase. The X-ray pattern for $B_{1\text{RevTilted}}$ is consistent with a 2D oblique lattice: one of the lattice parameters, c , is close to the d value. The lattice parameter a , that is related to the length of the layer fragment, increases on cooling, whereas the unit cell inclination angle, β slightly larger than 90°, is almost temperature independent as also shown in Fig. 1.

In order to examine the two mesophases observed in these compounds, we carried out miscibility studies between compound **11d-NCl-14** and the well-studied **14-NCl-14**.⁵⁻⁹ The reference compound has the following sequence of transitions: Cr. 116.5 °C $B_{1\text{RevTilted}}$ 127.7 °C SmAP_R 141.3 °C Iso. The binary phase diagram obtained is shown in Fig. 2. We can clearly see that the two phases of compound **11d-NCl-14** are completely miscible with the mesophases of the standard material over the entire composition range. It is noted that the temperature range of SmAP_R is broadened and lowered in the mixtures comparing to pure compounds.

Table 2 Phase transition temperatures ($^{\circ}\text{C}$) and corresponding enthalpies [J g^{-1}] for compounds of series III. Numbers at both sides of the sample names stand for the numbers of carbons in both end chains. N and Cl stand for substituents NO_2 and Cl at left and right wings, respectively. d stands for the existence of double bond(s)



Sample name	X	Y	Cr	$B_{1\text{RevTilted}}$	SmAP_R	Iso	ΔT (SmAP_R)
11-NCl-11d	NO_2	Cl	•	120.76 [10.95]	•	•	—
12-NCl-11d	NO_2	Cl	•	119.37 [0.61]	•	•	3.66
14-NCl-11d	NO_2	Cl	•	118.50 [0.90]	•	•	6.39
16-NCl-11d	NO_2	Cl	•	118.50 [0.95]	•	•	9.47
18-NCl-11d	NO_2	Cl	•	117.10 [0.99]	•	•	12.67
11d-NCl-14	NO_2	Cl	•	115.83 [0.85]	•	•	9.53
11d-NCl-11d	NO_2	Cl	•	105.97 [7.78]	•	•	—
11d-ClCl-11d	Cl	Cl	•	106.10 [12.04]	•	•	—
11d-NN-11d	NO_2	NO_2	•	149.77 [50.31]	•	•	—

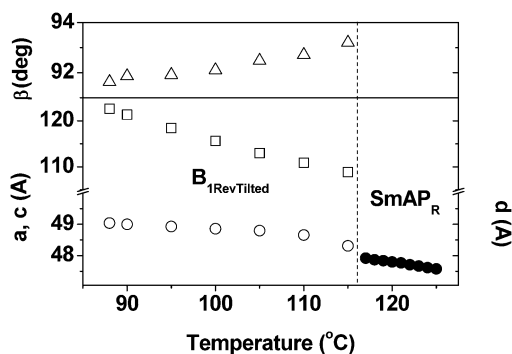


Fig. 1 Variation of layer spacing d in the SmAP_R phase of **11d-NCl-14** compound (solid circles) and parameters of 2D primitive unit cell in the $B_{1\text{RevTilted}}$ phase: a (open squares), c (open circles) and angle β (open triangles).

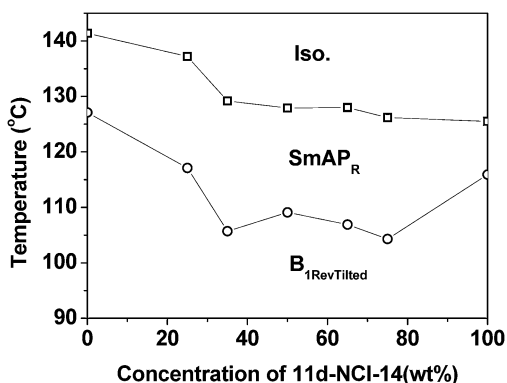


Fig. 2 Binary phase diagram obtained for a mixture of compound **14-NCl-14** and **11d-NCl-14**. In the mixtures, the SmAP_R temperature range becomes broader compared with those of pure compounds. The continuous line is drawn as a guide to the eyes.

To study the electrooptic switching properties of the mesophases in these compounds, we carried out experiments using a triangular wave electric field. ITO-coated glass plates were

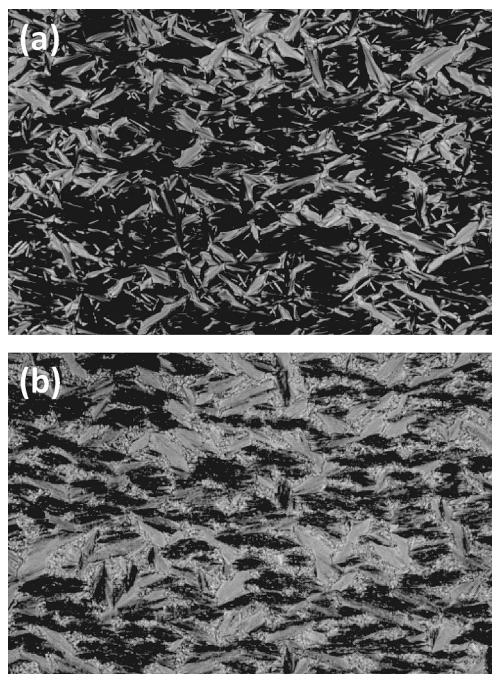


Fig. 3 Photomicrographs ($\times 200$) of textures of **11d-NCl-14** (a) at 123°C (SmAP_R phase) and (b) at 101°C ($B_{1\text{RevTilted}}$ phase). Cell thickness $5\ \mu\text{m}$.

treated with a polyimide (AL1254) and cured at 180°C . Both plates were rubbed antiparallel to each other for homogeneous alignment of the compound. An $8.4\ \mu\text{m}$ thick cell was filled with **11d-NCl-14** in the isotropic phase by capillary action. Fig. 3(a) and (b) show optical photomicrographs taken in the SmAP_R and $B_{1\text{RevTilted}}$ phases, respectively. When this compound was sandwiched in a cell treated for homeotropic alignment and cooled from the isotropic phase, a dark view indicating the uniaxial SmA phase was observed (not shown). In a homogeneous cell at 120°C , one broad polarization current peak for each half cycle was obtained as shown in Fig. 4(a). The single, broad switching current peak is characteristic of the switching process in SmAP_R .⁶ The broadness of the peak indicates field-induced

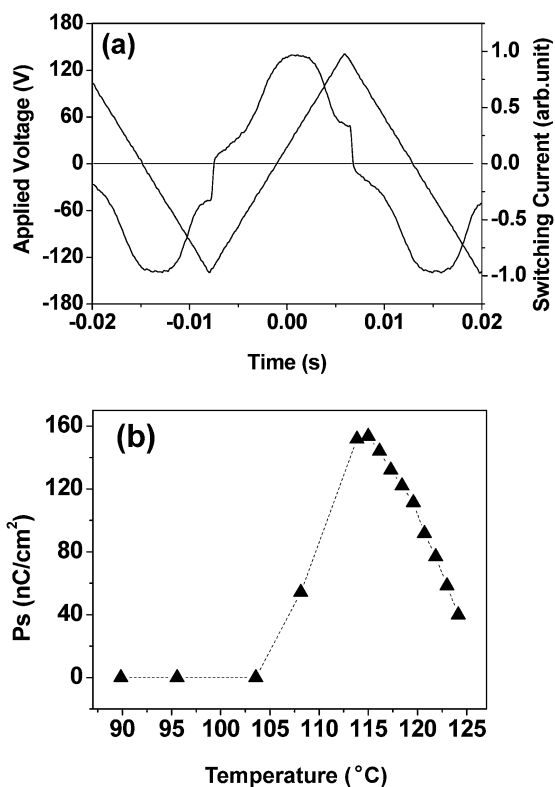


Fig. 4 (a) Polarization reversal current in the SmAP_R phase of **11d-NCl-14** at 120 °C under the application of a 280 V_{pp} triangular wave voltage of frequency 36 Hz; (b) P_s value as a function of temperature. The decrease of the P_s value in the B_{1RevTilted} phase is due to insufficient voltage to switch the polarization. Cell thickness 8.4 μm .

alignment of dipoles from a random orientation, through the Langevin process.^{8,9} In the SmAP_R phase the electric polarization, calculated from the integral of the switching peak, increases with lowering temperature (Fig. 4(b)) from ~ 40 nC/cm² at 124 °C to ~ 160 nC/cm² at 115 °C, which indicates growing polar order in this phase. The electric polarization decreases sharply in the B_{1RevTilted} phase, which is an artifact due to an insufficient field for breaking the antiferroelectric coupling in this phase.

The dielectric measurements were conducted in a planar, aligned cell. Since below 10 Hz there is a strong ion contribution to the dielectric response and the cut-off frequency for used ITO cells is ~ 1 MHz, the dielectric measurements were limited to a frequency range 10 Hz–1 MHz. Only a single relaxation mode was observed in the whole temperature range of liquid crystal phases. At each temperature the relaxation frequency and mode strength were obtained by fitting experimental points to the Cole–Cole formula; the parameter α which indicates the distribution of relaxation frequencies for the dielectric mode was close to 0 except for in temperature range near the phase transition where it increases to 0.4. The real part of the dielectric permittivity (ϵ') as a function of frequency for the compound **11d-NCl-14**, at various temperatures is shown in Fig. 5. In the SmAP_R phase the dielectric relaxation frequency increases from 70 to 440 Hz (Fig. 6) and the value of dielectric permittivity decreases from 60 to 20, with rising temperature. The high dielectric response with low relaxation frequency indicates the presence of a strong

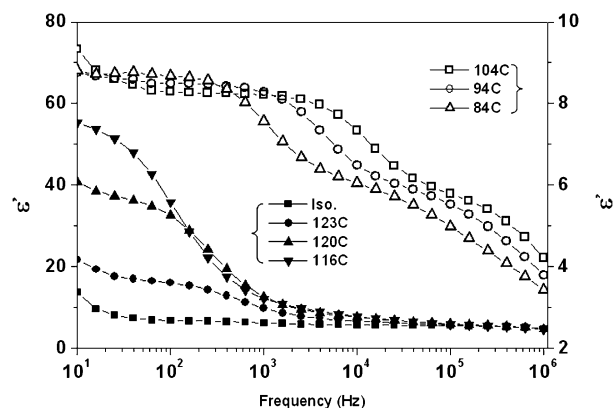


Fig. 5 The real part of the dielectric permittivity (ϵ') in the SmAP_R and B_{1RevTilted} phases of **11d-NCl-14** as a function of frequency at various temperatures. Solid symbols correspond to the data in the SmAP_R phase (left vertical scale) and the open symbols correspond to the data in the B_{1RevTilted} phase (right vertical scale). The continuous lines are the fits to the Cole–Cole formula. The high frequency mode is an artifact due to the limited conductivity of ITO electrodes; this mode also exists in the SmAP_R phase.

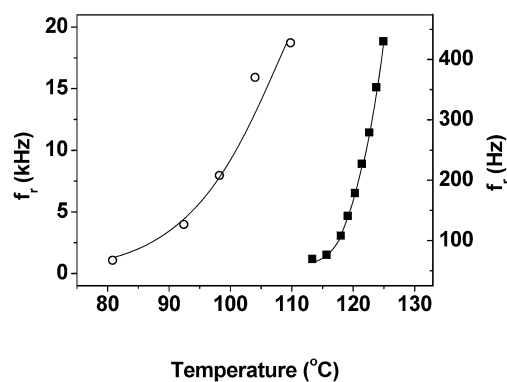


Fig. 6 Variation of relaxation frequency in the SmAP_R (left vertical scale) and B_{1RevTilted} phases (right vertical scale) of **11d-NCl-14** as a function of temperature. Cell thickness 8.4 μm . The continuous lines are drawn as a guide to the eyes.

positive dipolar correlation and dipole cooperative motions in the SmAP_R phase, which can be thought of as ferroelectric short range order in this phase. As indicated by dielectric measurement results this ferroelectric order of dipoles becomes weaker with increasing temperature.

In the B_{1RevTilted} phase the dielectric permittivity is one order of magnitude weaker and the dielectric relaxation frequency much higher than in the SmAP_R phase. The relatively small value of the dielectric constant in the B_{1RevTilted} phase indicates the antiferroelectric nature of this phase (Fig. 5). In the B_{1RevTilted} phase that is built of layer fragments, in which molecules are tilted from the layer normal and polarly ordered, the relaxation mode can be ascribed to fluctuation in the azimuthal orientation of the molecules in the layer fragments. Therefore this mode can be considered as an analogue of the antiphase azimuthal mode in the antiferroelectric SmC_A* phase made of calamitic or bent-core molecules. Observation of such a mode in a broken-layer

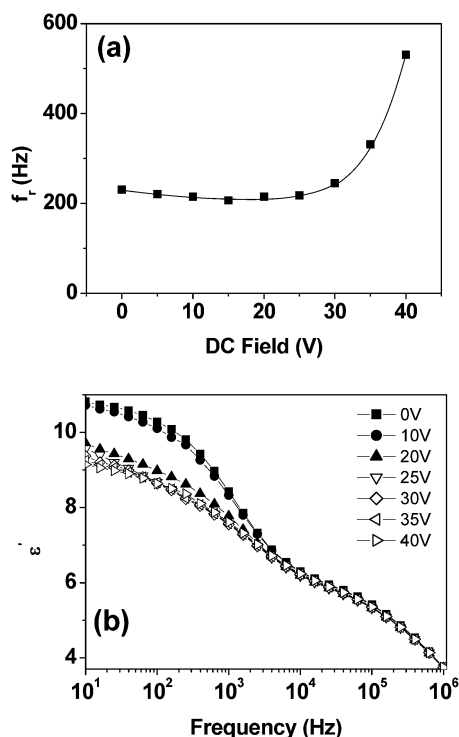


Fig. 7 Effect of DC bias voltage on the dielectric relaxation mode in (a) the SmAP_R phase (119 °C) and (b) the B_{1RevTilted} phase (94 °C) of **11d-NCI-14**. The relaxation frequency becomes higher with DC bias voltage in the SmAP_R phase. The dielectric response is suppressed by the DC bias voltage in the B_{1RevTilted} phase. Cell thickness 8.4 μm. The continuous lines are drawn as a guide to the eyes. The high frequency mode is an artifact due to limited conductivity of ITO electrodes.

columnar phase has already been reported by Gorecka *et al.*¹¹ However since the dielectric response in the B_{1RevTilted} phase is much weaker and at higher frequency than in the antiferroelectric lamellar B₂ phase,¹² we can assume that azimuthal fluctuation of molecules must be strongly suppressed, most probably due to some anchoring of the director at boundaries of the layer fragments. The effect of DC bias on the relaxation mode was also examined (Fig. 7(a)). In the SmAP_R phase it is noted that the relaxation frequency begins to rise keeping the dielectric strength the same in the field beyond 3 Vμm⁻¹. This might be expected, as under DC bias the collective motion of the dipoles is faster due to the enhanced correlation length and hence the relaxation frequency is increased. At still higher bias field the relaxation mode strength should be completely suppressed. However, full suppression was not observed due to the insufficient applied bias, limited by the equipment used in the experiment. Similar field dependent behaviour in the kHz frequency range was previously described by Shimbo *et al.*⁸ However, in the compound studied here the relaxation was observed in the lower frequency range, probably due to the higher viscosity of the material, as the SmAP_R phase is observed at lower temperatures.

3. Experimental

The molecular structures of the synthesized compounds were confirmed by the following analytical methods. Infrared (IR)

spectra were obtained using a JASCO FTIR-460 PLUS spectrometer. The carbon nuclear magnetic resonance (¹³C NMR) spectra were recorded on Varian Unity Plus spectrometer operating at 75 MHz, whereas ¹H NMR spectra were recorded at 300 MHz. Tetramethylsilane was used as an internal standard. Chemical shifts were reported in ppm. Thin layer chromatography (TLC) analyses were performed on Merck 60 F₂₅₄ silica gel aluminium plates. Column chromatography was carried out at atmospheric pressure using silica gel (100–200 mesh, Merck). Compositions of the synthesized compounds were determined by elemental analysis. Phase transition temperatures and associated enthalpies were determined by differential scanning calorimetry (Pyris Diamond Perkin-Elmer 7) at rates of 1–10 °C/min under cooling and heating runs. Texture observation and the identification of the mesophases were done using a polarizing optical microscope (Olympus, BX50) equipped with a hot stage and temperature controller (Mettler Toledo FP 82). Electrooptical switching behaviour was observed using a function generator connected with a high voltage amplifier. The polarization reversal current was measured by the standard triangular wave technique.¹³ The current was measured across a 1 MΩ resistance and the spontaneous polarization value was obtained by integrating the area under the curve. The dielectric measurement was conducted in a planar aligned cell with an indium tin oxide (ITO)-coated electrode. A frequency response analyzer (Solatron 1255B) with a dielectric interface Solatron (1296) and a Mettler temperature controller were used for this experiment.

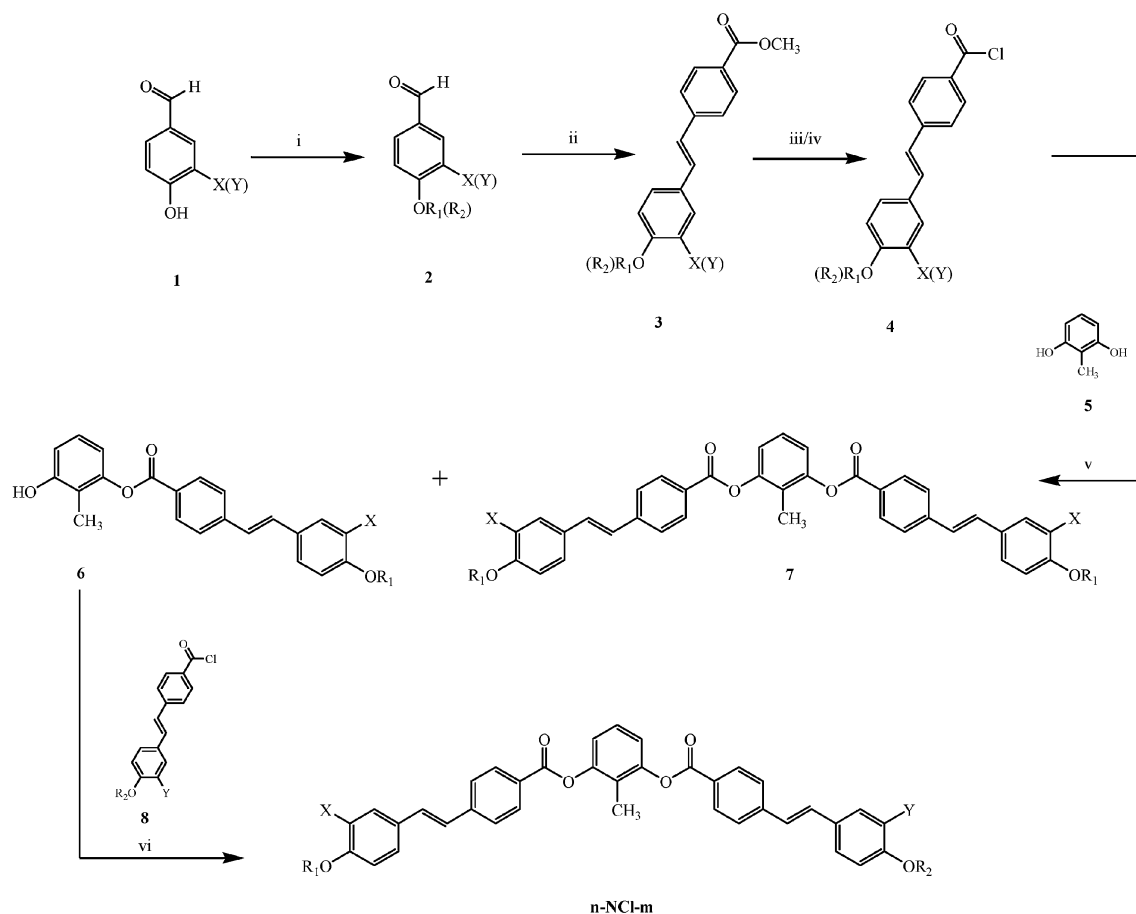
The synthesis of novel bent-core compounds was achieved by following the route depicted in Scheme 1.

3-Chloro-4-hydroxybenzaldehyde, 4-hydroxy-3-nitrobenzaldehyde, 11-bromo-1-undecene, 1-bromoundecane, 1-bromododecane, 1-bromotetradecane, 1-bromohexadecane, 1-bromooctadecane, 2-methylresorcinol, DMAP and 18-crown-6, was used as received from TCI (Tokyo Kasei Kogyo Co, Ltd), Aldrich and Wako. Alkoxy aldehyde **2** was prepared from hydroxyaldehyde **1** and the appropriate alkyl bromide or alkenyl bromide using Williamson etherification, and then was applied in a Wittig reaction with methyl 4-(triphenylphosphoniummethyl)benzoate bromide. The obtained stilbene derivative **3** after transformation into benzoic acid chloride **4**, followed by esterification reaction with resorcinol derivatives **5** gave a mixture of monosubstituted **6** and disubstituted **7** products, which were separated by column chromatography. Disubstituted products **7** were examined for mesomorphic properties, while mono-derivatives **6** were treated with the appropriate benzoic acid chloride, which resulted in the formation of asymmetrical bent-core compounds n-NCI-m.

Synthesis of 3-chloro-4-undec-10-enyloxybenzaldehyde **2**

A mixture of 3-chloro-4-hydroxybenzaldehyde **1** (10 g, 64 mmol), K₂CO₃ (11.5 g, 83 mmol), KI (13.8 g, 83 mmol) and 11-bromo-1-undecene (15.4 ml, 70 mmol) in DMF (200 ml) was heated at 80 °C for 8–10 h. Then water was added and the product was extracted with toluene (3 × 20 ml), and the organic phase was dried over MgSO₄. The solvent was evaporated and the crude product was crystallized several times from ethanol. Yield 70%.

2: NMR: δ_H (300 MHz, CDCl₃) 9.84 (s, 1H, CHO), 7.91 (s, 1H, Ar), 7.75 (dd, J₁ = 8.4 Hz, J₂ = 2.1 Hz, 1H, Ar), 7.02 (d,



Series I **12-NCl-m** $n = 12$; $m = 5, 7, 8, 10-16, 18$

Series II **14-NCl-m** $n = 14$; $m = 13-16$

Series III **n-NCl-11d** $m = 11$; $n = 11, 12, 14, 16, 18$

11d-NCl-14, 11d-NCl-11d, 11d-ClCl-11d, 11d-NN-11d

$X = \text{NO}_2$, $Y = \text{Cl}$

$R_1, R_2 = -\text{C}_n\text{H}_{2n\pm 1}$; $-\text{C}_m\text{H}_{2m\pm 1}$

Scheme 1 Synthetic route for the preparation of symmetric and asymmetric bent-core molecules for series I–III: i) $R_1(R_2)\text{Br}$, K_2CO_3 , KI, DMF; ii) methyl 4-(triphenylphosphoniummethyl)-benzoate bromide, CH_2Cl_2 , THF, 18-crown-6; iii) KOH/EtOH ; iv) $(\text{COCl})_2/\text{toluene}$; v) TEA, THF, DMAP, room temp., 4–5 h; vi) TEA, THF, DMAP, reflux 8 h.

$J = 8.4$ Hz, 1H, Ar), 5.86–5.75 (m, 1H, $\text{CH}=\text{CH}_2$), 5.03–4.91 (m, 2H, $\text{CH}=\text{CH}_2$), 4.12 (t, $J = 6.3$ Hz, 2H, OCH_2CH_2), 2.05–2.01 (m, 2H, CH_2), 1.90–1.83 (m, 2H, CH_2), 1.53–1.31 (m, 12H, CH_2); $\delta_{13\text{C}}$ (75 MHz, CDCl_3) 189.66, 159.43, 139.12, 131.16, 130.40, 129.92, 123.85, 114.10, 112.37, 69.45, 33.74, 29.39, 29.33, 29.19, 29.04, 28.85, 28.79, 25.81. IR (KBr): $\nu_{\text{max}}/\text{cm}^{-1}$, 2918, 2851, 1683, 1596, 1499, 1322, 1287, 1056, 918. Elemental analysis calc. (%) for $\text{C}_{18}\text{H}_{25}\text{ClO}_2$ (308.15): C, 70.00, H, 8.16, Cl, 11.48; found C, 69.59, H, 8.14, Cl, 11.65.

All alkoxy derivatives were synthesized using a similar procedure.

Synthesis of 4-*(E)*-2-[3-chloro-4-(undec-10-enyloxy)phenyl]ethenyl]benzoic acid methyl ester 3

To a solution of methyl 4-(triphenylphosphoniummethyl)-benzoate bromide (5.89 g, 12 mmol), dissolved in dry methyl chloride (70 ml) and tetrahydrofuran (100 ml), anhydrous

potassium carbonate (8.4 g, 61 mmol) followed by 18-crown-6 (20 mg, 0.07 mmol) were added. The reaction mixture was stirred at room temperature for 1 h. 3-Chloro-4-undec-10-enyloxybenzaldehyde (5.56 g, 18 mmol) was added to the yellow reaction mixture which was heated under reflux for 20 h. After filtration of inorganic salts, the reaction mixture was evaporated to dryness and ethanol was added to the oily residue, which led to the crystallization of product **3**. According to the spectral data, only (*E*)-stilbene was crystallized from the reaction mixture. Yield 45%.

3: NMR: δ_{H} (300 MHz, CDCl_3) 8.01 (d, $J = 8.4$ Hz, 2H, Ar), 7.56 (d, $J = 2.4$ Hz, 1H, Ar), 7.52 (d, $J = 8.1$ Hz, 2H, Ar), 7.33 (dd, $J_1 = 8.7$ Hz, $J_2 = 2.4$ Hz, 1H, Ar), 7.03 (q, $J = 16.5$ Hz, 2H, $\text{CH}=\text{CH}$), 6.89 (d, $J = 8.7$ Hz, 1H, Ar), 5.86–5.77 (m, 1H, $\text{CH}=\text{CH}_2$), 5.02–4.90 (m, 2H, $\text{CH}=\text{CH}_2$), 4.04 (t, $J = 6.6$ Hz, 2H, OCH_2CH_2), 3.92 (s, 3H, OCH_3), 2.05–2.00 (m, 2H, CH_2), 1.86–1.79 (m, 2H, CH_2), 1.51–1.24 (m, 12H, CH_2). δ_{C} (75 MHz, CDCl_3) 166.83, 154.55, 141.71, 139.20, 130.18, 130.02, 129.52, 128.76, 128.10, 126.50, 126.41, 126.12, 123.34, 114.11, 113.18, 69.23, 52.04, 33.78, 29.45, 29.38, 29.28, 29.09, 29.03, 28.90, 25.90. IR (KBr): $\nu_{\text{max}}/\text{cm}^{-1}$, 2924, 2852, 1713, 1593, 1501, 1469, 1284, 1192, 1108, 970. Elemental analysis calc. (%) for $\text{C}_{27}\text{H}_{33}\text{ClO}_3$ (440.21): C, 73.53, H, 7.54, Cl, 8.04; found C, 73.15, H, 7.60, Cl, 7.95

All stilbene derivatives were synthesized using a similar procedure.

Synthesis of 4-*{(E)-2-[3-chloro-4-(undec-10-enyloxy)phenyl]ethenyl}benzoic acid chloride 4*

To the solution of 4-*{(E)-2-[3-chloro-4-(undec-10-enyloxy)phenyl]ethenyl}benzoic acid methyl ester* (3 g, 6.81 mmol) in ethanol (200 ml), a solution of potassium hydroxide (1.15 g, 20.4 mmol) in ethanol (15 ml) was added and the mixture was heated under reflux for 10–12 h. After cooling the solution, crude product precipitated as a potassium salt. After drying under vacuum over sodium hydroxide, the obtained salt was suspended in toluene (200 ml) and treated with an excess of oxalyl chloride (5 ml). The reaction mixture was heated under reflux for 8 h. After filtration of the precipitated potassium chloride, the remaining solution was evaporated to dryness. The product slowly solidified at room temperature with a yield of 98%.

All benzoic acid chlorides were synthesized using a similar procedure.

Synthesis of 2-methyl-1,3-*{[4-*{(E)-2-[4-(dodecyloxy)-3-nitrophenyl]-1-ethenyl}benzoyloxy]methyl}benzyl-4-*{(E)-2-[3-chloro-4-(undec-10-enyloxy)phenyl]-1-ethenyl}benzoate 12-NCl-11d***

To a solution of 2-methylresorcinol (1.2 g, 9.67 mmol), triethylamine (1 ml, 7.13 mmol) and DMAP (20 mg, 0.16 mmol) in tetrahydrofuran (100 ml), 4-*{(E)-2-[3-chloro-4-(undec-10-enyloxy)phenyl]ethenyl}benzoic acid chloride 4* (0.86 g, 1.93 mmol) in dichloromethane (30 ml) was added dropwise. The reaction mixture was stirred at room temperature for 4–5 h, then the solvent was evaporated to dryness under reduced pressure. The obtained mixture of monosubstituted **6** and disubstituted **7** products was separated by column chromatography using silica

gel eluted with 0.5% of methanol in toluene. The disubstituted product was crystallized from ethyl acetate. Yield of monosubstituted derivative = 40%, disubstituted = 30%. To the mixture monosubstituted derivative **6** (0.40 g, 0.75 mmol), triethylamine (1 ml, 7.13 mmol), tetrahydrofuran (100 ml), DMAP (20 mg, 0.16 mmol), *{(E)-2-[4-nitro-3-(dodecyloxy)phenyl]ethenyl}benzoic acid 4* (0.42 g, 0.90 mmol) were added and the mixture was kept under reflux for 8 h. The asymmetric final product **12-NCl-11d** was purified by column chromatography and double recrystallization from ethyl acetate. Yield of **12-NCl-11d** = 20% The range of yields of this step varied from 20–40%.

All asymmetrical products were synthesized using the same procedure.

6: NMR: δ_{H} (300 MHz, DMSO) 9.60 (s, 1H, Ar–OH), 8.10 (d, $J = 8.4$ Hz, 2H, Ar), 7.77–7.74 (m, 3H, Ar), 7.55 (dd, $J_1 = 8.7$ Hz, $J_2 = 1.8$ Hz, 1H, Ar), 7.34 (q, $J = 16.2$ Hz, 2H, $\text{CH}=\text{CH}$), 7.14 (d, $J = 8.4$ Hz, 1H, Ar), 7.05 (t, $J = 8.1$ Hz, 1H, Ar), 6.75 (d, $J = 8.1$ Hz, 1H, Ar), 6.38 (d, $J = 7.8$ Hz, 1H, Ar), 5.83–5.70 (m, 1H, $\text{CH}=\text{CH}_2$), 4.99–4.88 (m, 2H, $\text{CH}=\text{CH}_2$), 4.05 (t, $J = 6.3$ Hz, 2H, OCH_2CH_2), 2.07–1.87 (m, 5H, Ar– CH_3 , CH_2), 1.76 (m, 2H, CH_2), 1.42–1.13 (m, 12H, CH_2); δ_{C} (75 MHz, DMSO) 164.01, 156.49, 153.93, 150.13, 142.66, 138.84, 130.24, 130.15, 130.08, 127.88, 127.24, 127.17, 126.62, 126.33, 126.22, 121.87, 116.78, 114.63, 113.83, 112.67, 68.66, 40.33, 40.05, 39.77, 39.50, 39.22, 38.94, 38.66, 33.20, 28.95, 28.79, 28.66, 28.51, 28.30, 25.39, 9.13. IR (KBr): $\nu_{\text{max}}/\text{cm}^{-1}$, 3348, 2927, 2851, 1692, 1593, 1497, 1274, 1261, 1098. Elemental analysis calc. (%) for $\text{C}_{33}\text{H}_{37}\text{ClO}_4$ (532.24): C, 74.35, H, 7.00, Cl, 6.65; found C, 74.61, H, 6.89, Cl, 6.71.

7 (11d-ClCl-11d): NMR: δ_{H} (300 MHz, CDCl_3) 8.20 (d, $J = 8.4$ Hz, 4H, Ar), 7.63–7.60 (m, 6H, Ar), 7.39–7.35 (dd, $J_1 = 2.1$ Hz, $J_2 = 8.7$ Hz, 2H, Ar), 7.33–6.91 (m, 9H, Ar, $\text{CH}=\text{CH}$), 5.89–5.75 (m, 2H, $\text{CH}=\text{CH}_2$), 5.03–4.91 (m, 4H, $\text{CH}=\text{CH}_2$), 4.06 (t, $J = 6.6$ Hz, 4H, OCH_2CH_2), 2.12 (s, 3H, Ar– CH_3), 2.08–2.01 (m, 4H, CH_2), 1.90–1.81 (m, 4H, CH_2), 1.50–1.32 (m, 24H, CH_2); δ_{C} (75 MHz, CDCl_3) 164.35, 154.65, 150.29, 142.56, 139.18, 130.68, 130.05, 130.00, 128.15, 127.64, 126.54, 126.33, 126.27, 123.94, 123.33, 119.89, 114.11, 113.12, 69.19, 33.78, 29.45, 29.37, 29.28, 29.08, 29.01, 28.88, 25.89, 10.09. IR (KBr): $\nu_{\text{max}}/\text{cm}^{-1}$, 2924, 2853, 1723, 1593, 1507, 1260, 1103. Elemental analysis calc. (%) for $\text{C}_{59}\text{H}_{66}\text{Cl}_2\text{O}_6$ (942.06): C, 75.22, H 7.06, Cl, 7.53; found C, 74.96, H, 7.05, Cl, 7.78.

12-NCl-11d: NMR: δ_{H} (300 MHz, CDCl_3) 8.23–8.19 (m, 4H, Ar), 8.02 (d, $J = 2.4$ Hz, 1H, Ar), 7.69–7.59 (m, 6H, Ar), 7.36 (dd, $J_1 = 8.7$ Hz, $J_2 = 2.1$ Hz, 1H, Ar), 7.33–6.91 (m, 9H, Ar, $\text{CH}=\text{CH}$), 5.86–7.75 (m, 1H, $\text{CH}=\text{CH}_2$), 5.03–4.92 (m, 2H, $\text{CH}=\text{CH}_2$), 4.13 (t, $J = 6.3$ Hz, 2H, OCH_2CH_2), 4.06 (t, $J = 6.6$ Hz, 2H, OCH_2CH_2), 2.13 (s, 3H, Ar– CH_3), 2.06–2.02 (m, 2H, CH_2), 1.88–1.83 (m, 4H, CH_2), 1.50–1.27 (m, 30H, CH_2), 0.88 (t, $J = 6.6$ Hz, 3H, CH_2CH_3); δ_{C} (75 MHz, CDCl_3) 164.28, 152.25, 150.33, 150.28, 142.61, 141.97, 139.22, 132.07, 130.77, 130.71, 130.11, 130.03, 129.19, 128.86, 128.17, 127.92, 127.66, 126.37, 126.30, 123.96, 123.45, 123.38, 114.67, 114.11, 113.17, 69.88, 69.27, 33.80, 31.90, 29.62, 29.56, 29.49, 29.46, 29.38, 29.34, 29.29, 29.26, 29.09, 29.02, 28.90, 25.91, 25.80, 22.68, 14.12, 10.11. IR (KBr): $\nu_{\text{max}}/\text{cm}^{-1}$, 2923, 2853, 1732, 1723, 1603, 1592, 1535, 1262, 1231, 1104, 1081. Elemental analysis calc. (%) for $\text{C}_{60}\text{H}_{70}\text{ClNO}_8$ (954.63): C, 74.40, H 7.28, N, 1.45, Cl, 3.66; found C, 74.30, H, 7.06, N, 1.46, Cl, 3.57.

14-NCI-13: NMR: δ_{H} (200 MHz, CDCl_3) 8.17–8.24 (m, 4H, Ar), 8.02 (d, $J = 2.2$ Hz, 1H, Ar), 7.54–7.72 (m, 6H, Ar), 7.03–7.40 (m, 9H, Ar, $\text{CH}=\text{CH}$), 6.91 (d, $J = 8.2$ Hz, 1H, Ar), 3.90–4.00 (m; 4H, OCH_2CH_2), 2.12 (s, 3H, Ar- CH_3), 1.75–1.94 (m, 4H, CH_2), 1.26–1.70 (m, 42H, CH_2), 0.88 (t, $J = 6.0$ Hz, 6H, CH_2CH_3); δ_{C} (50 MHz; CDCl_3) 164.56, 164.45, 154.88, 152.41, 150.53, 150.47, 142.79, 142.15, 132.24, 130.91, 130.87, 130.28, 130.19, 129.36, 129.02, 128.35, 128.32, 128.04, 127.82, 126.75, 126.54, 126.43, 126.43, 124.12, 123.6, 123.54, 114.84, 113.34, 70.04, 69.41, 32.09, 29.89, 29.85, 29.77, 29.70, 29.55, 29.46, 29.24, 29.10, 26.11, 26.02, 22.87, 14.32, 14.14, 10.18. IR (KBr): $\nu_{\text{max}}/\text{cm}^{-1}$: 2922, 2852, 1735, 1603, 1534, 1467, 1266, 1231, 1104. Elemental analysis calc. (%) for $\text{C}_{64}\text{H}_{80}\text{ClNO}_8$ (1025.56): C, 74.86, H, 7.85, N, 1.36, Cl, 3.45; found C, 74.50, H, 7.90, N, 1.45, Cl, 3.30.

4. Conclusions

The mesomorphic behaviour of several asymmetric bent-core compounds derived from 2-methylresorcinol, containing a lateral chloro/nitro group and saturated or unsaturated terminal alkoxy chain/s, has been investigated. The mesophases exhibited by these compounds have been characterized as the lamellar uniaxial polar SmA phase (SmAP_R) and the broken-layer type columnar $\text{B}_{1\text{RevTilted}}$ phase. The cross-section of the block forming the $\text{B}_{1\text{RevTilted}}$ phase contains 20–30 molecules. Introduction of a double bond in the terminal end chain lowers the isotropization temperatures but also slightly destabilizes the smectic phase. A similar observation was reported by Achten *et al.*¹⁴ The dielectric relaxation in the SmAP_R phase is much stronger than in the $\text{B}_{1\text{RevTilted}}$ phase due to the cooperative dipolar relaxation. In the antiferroelectric $\text{B}_{1\text{RevTilted}}$ phase the dielectric response arises from weak anti-phase fluctuation of the polarization vector in neighbouring layer fragments.

Acknowledgements

This work is partly supported by a Grant-in-Aid for Scientific Research (S) (16105003) from the Ministry of Education, Culture, Science, Sports and Technology of Japan. K. G. and

S. D. are respectively supported by Japan Society for Promotion of Science and the DST, Govt. of India for the project number SR/FTP/PS-48/2006 under the SERC Fast Track Scheme.

References

- 1 H. Takezoe and Y. Takanishi, *Jpn. J. Appl. Phys. A*, 2006, **45**, 597; R. Amaranatha Reddy and C. Tschierske, *J. Mater. Chem.*, 2006, **16**, 907; J. Mieczkowski and J. Matraszek, *Polish J. Chem.*, 2005, **79**, 179; J. Etxebarría and M. Blanca Ros, *J. Mater. Chem.*, 2008, **18**, 2919.
- 2 T. Niori, T. Sekine, J. Watanabe, T. Furukawa and H. Takezoe, *J. Mater. Chem.*, 1996, **6**, 1231; D. R. Link, G. Natale, R. Shao, J. E. MacLennan, N. A. Clark, E. Korblova and D. M. Walba, *Science*, 1997, **278**, 1924.
- 3 B. K. Sadashiva, R. Amaranatha Reddy, R. Pratibha and N. V. Madhusudana, *Chem. Commun.*, 2001, 2140; B. K. Sadashiva, R. Amaranatha Reddy, R. Pratibha and N. V. Madhusudana, *J. Mater. Chem.*, 2002, **12**, 943.
- 4 A. Eremin, S. Diele, G. Pelzl, H. Nadasi, W. Weissflog, J. S. Salfetnikova and H. Kresse, *Phys. Rev. E*, 2001, **64**, 051707; H. N. Shreenivasa Murthy and B. K. Sadashiva, *Liq. Cryst.*, 2004, **31**, 567.
- 5 J. Mieczkowski, K. Gomola, J. Koseska, D. Pocięcha, J. Szydłowska and E. Gorecka, *J. Mater. Chem.*, 2003, **13**, 2132.
- 6 D. Pocięcha, M. Cepic, E. Gorecka and J. Mieczkowski, *Phys. Rev. Lett.*, 2003, **91**, 185501.
- 7 D. Pocięcha, N. Vaupotic, E. Gorecka, J. Mieczkowski and K. Gomola, *J. Mater. Chem.*, 2008, **18**, 881.
- 8 Y. Shimbo, E. Gorecka, D. Pocięcha, F. Araoka, M. Goto, Y. Takanishi, K. Ishikawa, J. Mieczkowski, K. Gomola and H. Takezoe, *Phys. Rev. Lett.*, 2006, **97**, 113901.
- 9 Y. Shimbo, Y. Takanishi, K. Ishikawa, E. Gorecka, D. Pocięcha, J. Mieczkowski, K. Gomola and H. Takezoe, *Jpn. J. Appl. Phys.*, 2006, **45**, L282.
- 10 J. Szydłowska, J. Mieczkowski, J. Matraszek, D. W. Bruce, E. Gorecka, D. Pocięcha and D. Guillon, *Phys. Rev. E*, 2003, **67**, 031702.
- 11 E. Gorecka, N. Vaupotic, D. Pocięcha, M. Cepic and J. Mieczkowski, *ChemPhysChem*, 2005, **6**, 1087.
- 12 D. Pocięcha, E. Gorecka, M. Cepic, N. Vaupotic, K. Gomola and J. Mieczkowski, *Phys. Rev. E*, 2005, **72**, 060701.
- 13 K. Miyasato, S. Abe, H. Takezoe, A. Fukuda and E. Kuze, *Jpn. J. Appl. Phys.*, 1983, **22**, L661.
- 14 R. Achten, A. Koudijs, M. Giesbers, A. T. M. Marcelis and E. J. R. Sudholter, *Liq. Cryst.*, 2005, **32**, 277.